

Design and Characterization of Biocomposites from Poly(lactic acid) (PLA) and Buriti Petiole (*Mauritia flexuosa*)

Samantha Andrade Vale de Sousa¹, Mercês Coelho da Silva², Orlando Gama da Silva Júnior³, Artur Caron Mottin⁴, Rodrigo Lambert Oréface³ and Eliane Ayres^{1*}

¹Minas Gerais State University - UEMG, Department of Materials, Technologies and Processes, School of Design, Avenida Antônio Carlos, 7545, Belo Horizonte-MG, Brazil

²Department of Materials Engineering, Federal University of Itajubá – UNIFEI, Rua Irmã Ivone Drumond, 200 - Distrito Industrial II, Itabira - MG, Brazil

³Department of Metallurgical and Materials Engineering, Federal University of Minas Gerais – UFMG, Av. Pres. Antônio Carlos, 6627 - Pampulha, Belo Horizonte - MG, Brazil

⁴Mechanical Department, Minas Gerais Federal Institute – IFMG, Av. Michael Pereira de Souza, 3007, Avenue - Campinho - Congonhas - MG, Brazil

Received November 08, 2016; Accepted February 20, 2017

ABSTRACT: Buriti or miriti (*Mauritia flexuosa*) is a palm tree found in the Brazilian cerrado. Herein buriti petiole, part of the trunk that supports the leaves, was ground and used without any treatment as low density load to prepare poly(lactic acid) biocomposites. X-ray microtomography of buriti petiole showed its porous structure, with a wide pore size distribution determined with the aid of SEM. The obtained biocomposites with 1, 5 and 10 wt% of buriti petiole particles were investigated by their sessile drop contact angle, FTIR, TGA and tensile test. The tensile properties indicated poor adhesion between phases, which is crucial to optimize the biocomposite's performance. Further studies with fiber treatment are being planned.

KEYWORDS: Buriti petiole, porous structure, PLA, biocomposites

1 INTRODUCTION

Lignocellulosic fibers are widely studied as potential reinforcing fillers in polymer matrices for producing new eco-friendly materials. Only a few studies about buriti palm tree fibers used as composites are found because they are less well known and have only recently been investigated as possible composite reinforcement [1]. Buriti or miriti (*Mauritia flexuosa*) is a palm tree found in the north Amazonian region of Brazil. Two distinct fibers can be extracted from the buriti palm tree, one from the leaf and the other from the petiole part of the trunk that supports the leaves (Figure 1). Portela *et al.* [1] stated that buriti petiole fibers are very strong fibers, with tensile strength reaching 350 MPa. Santos *et al.* [2] reported yield stress and modulus in the range of 270 MPa and 10 GPa respectively for buriti fibers extracted from the palm tree leaves. An interesting characteristic of buriti petiole is its relatively low

moisture absorption and open porosity, in association with a density lower than 0.1 g cm^{-3} [3]. On the other hand, the density of buriti fibers obtained from the leaves was reported to be 1.31 g cm^{-3} [2]. This value is comparable with other lignocellulosic fibers such as coconut (1.15 g cm^{-3}), banana (1.35 g cm^{-3}), sisal (1.45 g cm^{-3}) and pineapple leaf (1.44 g cm^{-3}) [4]. Many people who live in the nearby islands of Guajará bay (Pará state) ensure their livelihood by cutting the petioles and crossing the bay by boat to sell them in the markets of Belém (capital of Pará). Once in the markets, they are transformed by the work of artisans into small handcrafted boats and sold at low price (Figure 1).

Environmental pollution due to nondegradable materials has steadily increased and packaging is a large part of the problem, mainly due to inappropriate disposal. Poly(lactic acid) (PLA) has played a central role in replacing fossil-based polymers and the use of PLA in packaging has largely increased over the last five years [5]. In this context, the current study aimed to prepare and characterize biocomposites of PLA and buriti petiole (BP), giving buriti petiole a more technological application and adding value to it.

*Corresponding author: eayres.pu@hotmail.com

DOI: 10.7569/JRM.2017.634115



Figure 1 (left) Illustration of buriti petiole; (right) photograph of the small handcrafted boats.

2 EXPERIMENTAL

2.1 Materials

The PLA filament (natural color and 1.75 mm diameter) from 3D GRAF was used. Buriti petiole (BP) was purchased in “Ver-o-Peso” market, a market hall in Belém, Brazil, located at Guajará Bay riverside.

2.2 Methods

First, BP was ground into a fine powder with the aid of a grinder (IKA A10, IKA Labortechnik, Germany) and passed through 325 mesh sieve. Composites of PLA/BP containing 1, 5 and 10 wt% of BP were prepared by melt mixing in a Haake Rheomix Polydrive R 600 (Thermo Fisher Scientific) at 180 °C and rotor speed of 40 rpm for 5 min. The films (0.50 mm) were produced by the conventional method of hot pressing (Sagec model sgpl) at 170 °C, first for 2 min at 1 MPa pressure, then for 2 min at 5 MPa, and finally for 1 min at 8 MPa. Biocomposite films prepared as described were named PLA/PB1%, PLA/PB5% and PLA/PB10%.

2.3 Characterizations

The morphology of BP was studied using X-ray microtomography (Skyscan 1174, Aartselaar, Belgium). The maximum peak voltage of the Skyscan 1174 X-ray source was 50 kV with a maximum power of 40 W (current of 800 μ A). The detection system consisted of a 14-bit cooled CCD camera coupled to a scintillator by lenses with 1:6 zoom ranges. While the sample was rotated, multiple 2D X-ray projections were taken every 0.7° rotation step over 360°. The 2D cross-sectional images were reconstructed as three-dimensional images with the aid of a specialized Skyscan software package.

The BP was analyzed via scanning electron microscopy (SEM) (Shimadzu model Vega 3LM) at an accelerating voltage of 10 kV. Samples for SEM were coated with gold using a sputter coater (SPI Sputter Coater,

SPI Supplies, PA, USA). BP mean pore size and pore size distribution were obtained from 100 individual measurements on SEM images by using image analysis software (Image J, National Institutes of Health, USA). Moreover, the total porosity was determined with the aid of a manual pycnometer for density analysis (Multipycnometer from Quantachrome Instruments).

The BP was analyzed on an X-ray diffractometer (Shimadzu, model XRD-7000) using monochromatic $\text{CuK}\alpha$ radiation ($\lambda = 1.54$) in the range of $2\theta = 5\text{--}40^\circ$ with a scanning rate of $0.1^\circ \text{ min}^{-1}$. The X-ray unit was operated at 45 kV and 40 mA.

Contact angle measurements were performed using the sessile drop technique with a Digidrop goniometer from GBX Instruments. The system was equipped with a CCD camera connected to a computer and to an automatic liquid dispenser. The contact angle was determined by placing a 6 μ L drop of water on the film surface using a syringe and images were immediately sent via the CCD camera to the computer for analysis. The results represent an average angle between the right and left angles. Three consecutive measurements were made at room temperature using the Surface Energy software mode, which allows direct measurement of contact angle (in degrees).

Fourier transform infrared (FTIR) experiments were performed with the aid of a Thermo Scientific Nicolet™ 6700 FT-IR spectrophotometer at a 4 cm^{-1} resolution and 256 co-added scans. The spectra were obtained using the ATR (attenuated total reflection) technique, in which the samples were pressed against a ZnSe crystal and spectra were collected from 650–4000 cm^{-1} .

The thermogravimetric analyses (TGA) were performed with small dry samples weighing around 10 mg using Seiko-SII Nanotechnology Inc. model Exstar 7200 equipment under nitrogen atmosphere (flow rate of 40 $\text{cm}^3 \text{ min}^{-1}$). Samples were heated from 25 °C to 800 °C at a 10 °C min^{-1} heating rate.

The PLA film and biocomposites were characterized for their tensile properties using an Instron testing machine (model EMIC 3000) with load cell of 200 N. Tensile properties were characterized according to ASTM D-638 and at least five specimens were tested to obtain the average values. A crosshead speed of 20 mm min^{-1} and a gage length of 13 mm were used for the tests.

3 RESULTS AND DISCUSSION

3.1 Buriti Petiole (BP)

Figure 2 shows the BP photography and three-dimensional image obtained by X-ray microtomography. The channels which form the BP inner porous structure can be observed, as already found in the literature [3].

An SEM micrograph and the corresponding histogram of BP are displayed in Figure 3. As can be seen, BP exhibits a wide pore size distribution with mean pore size in a range of $82 \pm 27 \mu\text{m}$.

The total porosity was found to be $86.7 \pm 0.02\%$ and was determined according to the method described by Donato and Lazzara [6] using Equation 1:

$$P(\%) = \frac{(\rho_a - \rho_r)}{\rho_a} \times 100 \quad (1)$$

where ρ_a is the apparent density determined by helium pycnometry and ρ_r is the relative density.

The BP XRD profile (Figure 4) shows three peaks around 16° , 22° and 34° , typical of cellulose I [7], corresponding to crystallographic planes (101), (002) and (040) respectively [8].

The fiber crystallinity index was estimated using Equation 2 defined by an empirical method [9]:

$$I_c = \frac{I_{(002)} - I_{(am)}}{I_{(002)}} \times 100 \quad (2)$$

where I_c = crystallinity index in percentage, $I_{(002)}$ = the diffraction intensity peak representing the crystalline

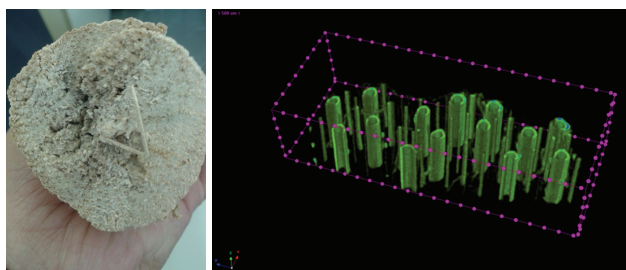


Figure 2 (left) Photograph of BP; (right) 3D image of BP obtained by X-ray microtomography.

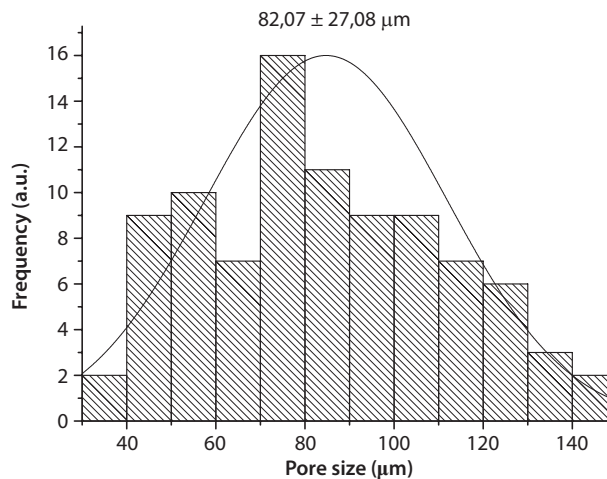
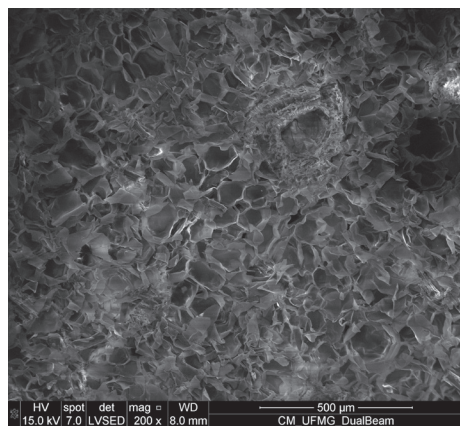


Figure 3 (left) SEM micrograph of BP; (right) statistical pore size (histogram) of BP.

material around $2\theta = 22^\circ$ and $I_{(am)}$ = diffraction intensity peak that represents the amorphous material around $2\theta = 16^\circ$.

According to Equation 2, the crystallinity index of BP was estimated to be 49%. This value is in accordance with a semicrystalline material and is mainly due to cellulose content, which is in the range of 51% [10].

3.2 Hydrophilic/Hydrophobic Properties of PLA and Biocomposite Films

The wettability of films was assessed by the contact angle (θ) measurements (Figure 5).

The value of $\theta = 76^\circ$ found for neat PLA is in accordance with the literature [11]. It was observed that when 1% of BP was incorporated, the film hydrophilicity was markedly increased (θ decreased from 76° to

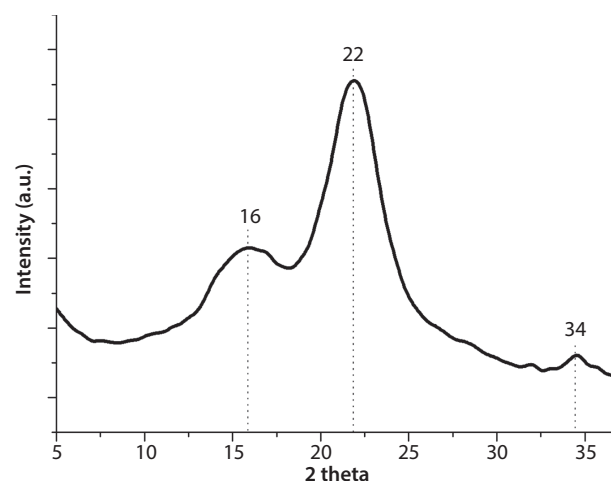


Figure 4 XRD intensity profile of buriti petiole (BP).

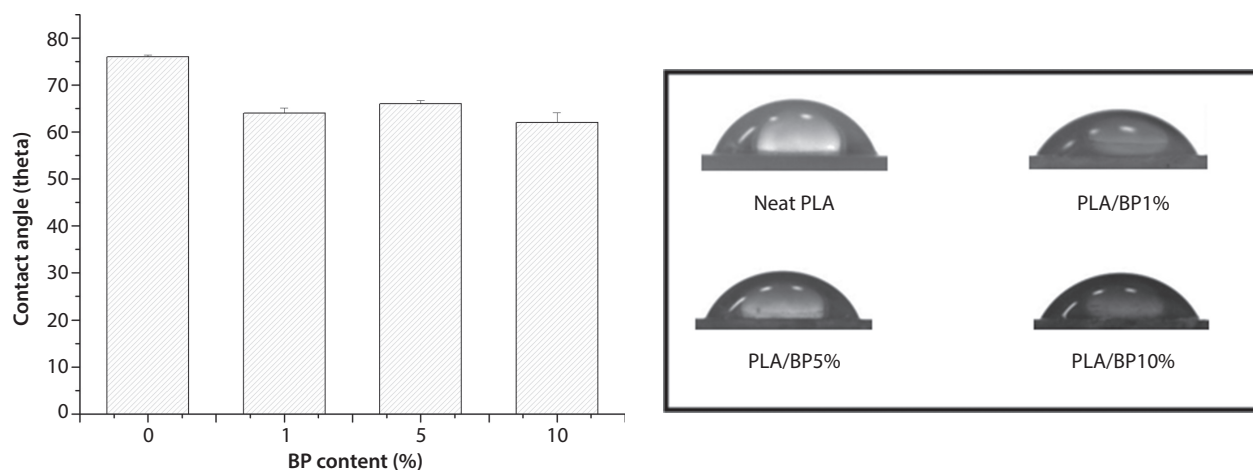


Figure 5 (left) Contact angle values of neat PLA and biocomposites; (right) images of sessile drops.

64°). This fact is probably due to the hydroxyl groups present in the chemical structure of the BP. With the increase of BP content to 5%, the value of the contact angle increased again ($\theta = 66^\circ$). This behavior might be accounted for, to some extent, by an increase in surface roughness, possibly due to BP agglomeration. For a flat hydrophobic surface ($\theta > 90^\circ$), θ increases with the increasing roughness.

Instead, for hydrophilic surfaces ($\theta < 90^\circ$), θ tends to decrease with the increasing roughness [12]. In other words, we might suggest the existence of two opposing factors contributing to change the wettability of the films. In the case of PLA/BP5%, the increase in roughness seems to be the predominating factor and might explain the increase in the contact angle. With 10% of BP content the contact angle ($\theta = 62^\circ$) decreased again, indicating that for higher contents of fiber the presence of hydrophilic entities predominates in the wettability behavior of the film. The decrease in the contact angle might also indicate low adhesion between BP and PLA matrix, that is, the hydroxyl groups of BP were available to interact with the water rather than with PLA.

3.3 Fourier Transform Infrared Spectroscopy (FTIR)

In order to investigate the occurrence of some interaction between the fibers and the PLA matrix, FTIR spectra of BP, neat PLA and PLA/BP10% were obtained and are shown in Figure 6.

Regarding the BP spectrum (Figure 6a), the stretching band can be seen at 3334 cm^{-1} , which is characteristic of O-H group present in the cellulose, lignin and hemicellulose [13]. The stretching band corresponding to CH linkage of CH and CH_2 groups present in cellulose and hemicellulose was observed at 2912 cm^{-1} [14]. The band at 1730 cm^{-1} is the characteristic band

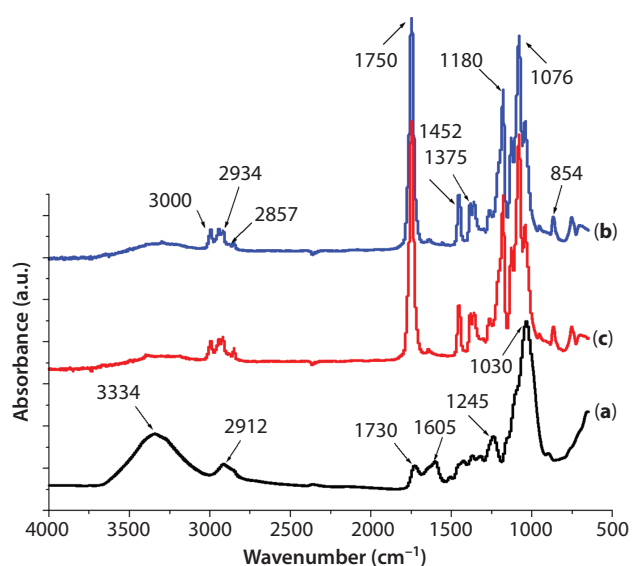


Figure 6 FTIR of (a) BP, (b) neat PLA and (c) PLA/BP10%.

of carbonyl ($\text{C}=\text{O}$) stretching due to the acetyl groups of hemicellulose and the band at 1605 cm^{-1} can be explained by the presence of moisture in the fibers [14]. Weak absorptions in the range of $1500\text{--}1350\text{ cm}^{-1}$ are reported to be due to the C-H bending and C-O stretching of hemicellulose, in addition to the C-OH in plane stretching of cellulose [15]. The band at 1245 cm^{-1} might be attributed to the vibration of C-O bonds of ethers, esters or phenolic groups of waxes and greases commonly found in lignocellulosic fibers [16].

The strong band with absorption peak at 1030 cm^{-1} may be associated with the C-O stretching of hydroxyl and ether groups in the cellulose [14]. In general, the FTIR spectrum of BP (Figure 6a) is a characteristic spectrum of lignocellulosic materials. A fairly detailed description of FTIR absorptions of the main

components of lignocellulosic materials has been presented by others [13].

In the case of neat PLA spectrum (Figure 6b), the bands' assignments are in accordance with the literature as follows: $\nu(\text{CH})$ stretch ($2900\text{--}3000\text{ cm}^{-1}$), $\nu(\text{C}=\text{O})$ ester carbonyl (1760 cm^{-1}), $\nu(\text{CH})$ deformation ($1350\text{--}1460\text{ cm}^{-1}$), $\nu(\text{CO})$ stretching ($1040\text{--}1270\text{ cm}^{-1}$), and $\nu(\text{C}-\text{C})$ stretching (870 cm^{-1}) [17]. It is possible to notice that the spectrum of PLA/BP10% (Figure 6c) is completely identical to that of PLA (Figure 6b). It is likely that, due to the similarity of the bands, overlapping has occurred. More interestingly, the band corresponding to O-H region present in the fiber cannot be seen. According to Thanki *et al.* [18], ATR-FTIR is used for the surface characterization but the intensity of the observed bands depends on the film thickness, among other parameters. As reported, surface segregation of methyl side groups at the surface is well influenced by the thickness of the films and it is significantly reduced in the case of thin films; for example, PLA films with thickness of $1\text{ }\mu\text{m}$ do not exhibit surface segregation of methyl side groups [18]. Thus, the fact that we have worked with thicker films might partially explain the absence of O-H band in the PLA/BP10% FTIR spectrum. However, this result was in disagreement with the contact angle measurements.

In order to confirm the presence of BP in the biocomposite, subtraction of PLA/BP10% and PLA spectra was performed as shown in Figure 7.

The subtraction spectrum (Figure 7b) closely resembles the BP spectrum (Figure 7a). The main difference between the spectra of Figure 7 is the absence of the O-H absorption band in the subtraction spectrum

(Figure 7b). In spite of this, such spectrum is indicative of BP in PLA/PB10% biocomposite.

3.4 Thermogravimetric Analysis (TGA)

Thermal stability of neat PLA, BP and biocomposites was evaluated by their thermogravimetric (TG) curves (Figure 8). The BP derivative thermogravimetric (DTG) curve is shown in the upper corner of Figure 8.

Figure 8a corresponds to the BP curve. According to the literature, fiber degradation occurs in four stages corresponding to the moisture evaporation, hemicellulose and cellulose degradation and decomposition

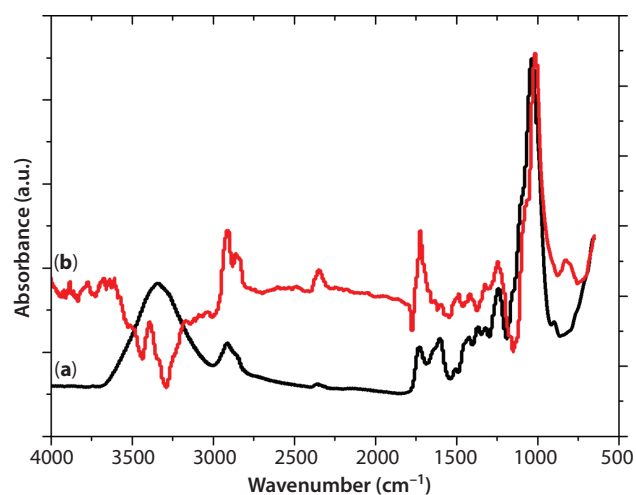


Figure 7 FTIR of (a) BP and (b) spectra subtraction (PLA/BP10%–PLA).

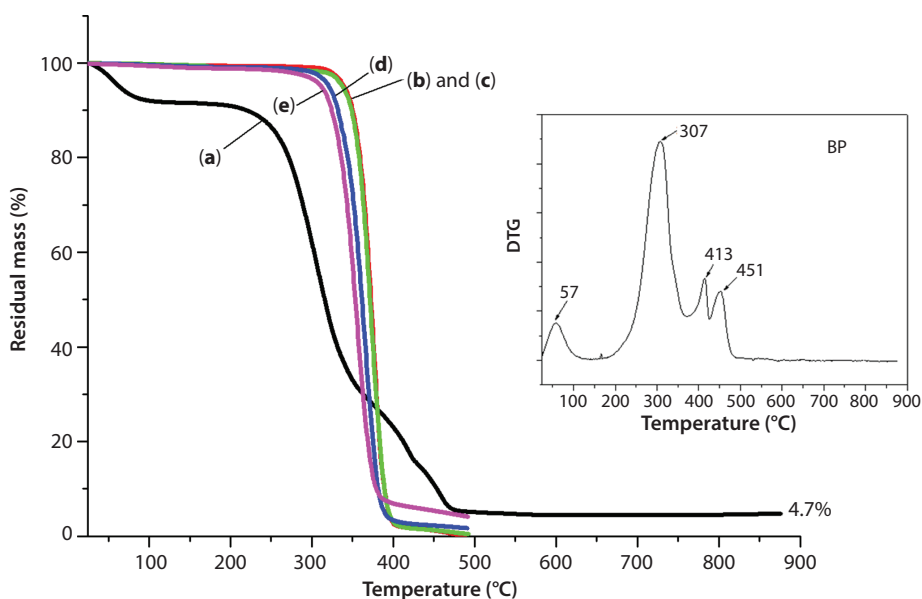


Figure 8 TG curves of (a) BP, (b) neat PLA, (c) PLA/BP1%, (d) PLA/BP5% and (e) PLA/BP10%.

of lignin [16]. In the BP DTG curve (upper corner), the moisture evaporation from the fiber appears around 57 °C. This result corroborates with those reported by others who also attributed moisture evaporation to an initial mass loss between 25 and 75 °C for buriti petiole [3]. The second event, with a maximum mass loss at 307 °C, occurs between 247 and 358 °C and may be related to the degradation of holocellulose (hemicellulose + cellulose) [19]. Cellulose is thermally more resistant than hemicellulose, probably due to its crystalline structure [20]. According to Kabir *et al.* [15], in their experiments with hemp fiber, cellulose was completely decomposed in the range of 240–350 °C, whereas hemicellulose had already been decomposed at 290 °C. The two peaks at 413 and 451 °C can be attributed to degradation of lignin that occurs in a very wide temperature range from 150 to 450 °C [15]. According to Gonçalves *et al.* [19], in their experiments with banana fiber, due to its complex structure it was not possible to observe the degradation of lignin, since it degrades with very small mass losses in a wide temperature range from 100 to 900 °C.

Monteiro *et al.* [3], upon analyzing the DTG curve of buriti petiole, have suggested that it is thermally more stable than the hemp and banana fibers. After complete degradation a solid residue corresponding to 4.7% of the material was left, probably carbon and metal oxides formed from the minerals present in vegetable fiber. The TG curve of neat PLA (Figure 8b) shows the degradation profile in a single stage, as has already been reported for neat PLA [21, 22]. Regarding the biocomposites, it can be observed that as the BP content increases, the thermal stability of composites decreases. All curves follow the same profile of PLA curve, that is, one stage for degradation. This was expected, since PLA is the main component and was homogeneously mixed with low contents of BP. Hence the behavior of PLA has predominated. The biocomposites showed an intermediate thermal behavior between PLA and BP. The same behavior was found by Awal *et al.* [23] in the TG analysis of PLA reinforced with cellulosic fibers. Likewise, Santos *et al.* [2] reported intermediate thermal behavior for composites obtained by adding buriti leaf fibers into thermosetting resin matrix. According to Jandas *et al.* [24], some studies have demonstrated that at high temperatures the presence of fibers deforms the crystalline structure of PLA and decreases their thermal stability.

3.5 Tensile Test

Figure 9 shows the tensile stress-strain curves of neat PLA and biocomposites. The tensile property values derived from the test are summarized in Table 1.

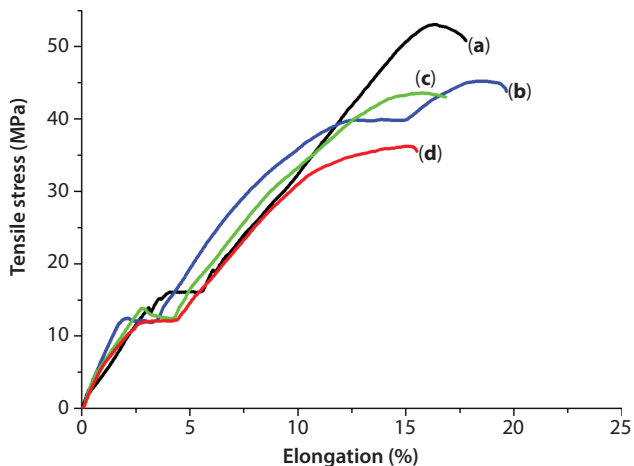


Figure 9 Tensile stress-strain curves of (a) neat PLA, (b) PLA/BP1%, (c) PLA/BP5% and (d) PLA/BP10%.

Table 1 Tensile properties of neat PLA and biocomposites.

Sample	Tensile strength (Mpa)	Elongation (%)
Neat PLA	51.17 ± 2.77	17.70 ± 14.71
PLA/BP1%	49.12 ± 2.00	19.64 ± 12.60
PLA/BP5%	43.08 ± 1.30	16.79 ± 2.19
PLA/BP10%	35.67 ± 1.92	15.45 ± 4.32

The tensile strength of the natural color PLA filament was reported to be 57 MPa [25]. This value is very close to the found value in this research. The value of the elongation, however, is well above the value found by these authors (2.35%), probably due to the presence of plasticizer in the filament.

The results show that the presence of BP has negatively affected the tensile strength of PLA. This is a strong indication that, in spite of homogeneous dispersion in the PLA matrix, BP had low adhesion with the matrix. Further studies involving surface modification of BP are needed in order to improve the interfacial adhesion between the polymeric matrix and BP.

4 CONCLUSIONS

Due to its high porosity, buriti petiole (BP) is interesting for use as low density filler. In this work, BP was ground into a fine powder and mixed without any treatment with PLA at 1, 5 and 10 wt%. FTIR analysis was inconclusive regarding the occurrence of interactions between chemical groups of PLA and BP. Tensile properties of the obtained biocomposites indicated poor adhesion between phases because neat PLA properties were not improved. Further studies

involving fiber treatment should be done in order to reach biocomposites with higher contents of BP and good performance in terms of mechanical properties. Due to its low density, BP is particularly attractive as filler and hence deserves to be better exploited.

ACKNOWLEDGMENTS

The authors gratefully acknowledge National Council for Scientific and Technological Development (CNPq) and Foundation for Research Support of Minas Gerais State (FAPEMIG) for the financial support and Coordination of Improvement of Senior Staff (CAPES) for the research studentship.

REFERENCES

1. T.G.R. Portela, L.L. da Costa, N.S.S. Santos, F.P.D. Lopes, and S.N. Monteiro, Tensile behavior of lignocellulosic fiber reinforced polymer composites: Part II buriti petiole/polyester. *Matéria (Rio J.)* **15**, 195–201 (2010).
2. R.S. Santos, A.A. Souza, M.A. De Paoli, and C.M.L. de Souza, Cardanol formaldehyde thermoset composites reinforced with buriti fibers: Preparation and characterization. *Composites Part A* **41**, 1123–1129 (2010).
3. S.N. Monteiro, R.J.S. Rodriguez, L.L. da Costa, T.G.R. Portela, and N.S.S. Santos, Thermal behavior of buriti biofoam. *Matéria (Rio J.)* **15**(2), 104–109 (2010).
4. K.G. Satyanarayana, K. Sukumaran, P.S. Mukherjee, and S.G.K. Pillai, Materials science of some lignocellulosic fibers. *Mettlography* **19**, 389–400 (1986).
5. E. Castro-Aguirre, E. Iñiguez-Franco, H. Samsudin, X. Fang, and R. Auras, Poly(lactic acid)—Mass production, processing, industrial applications, and end of life. *Adv. Drug Deliver. Rev.* **107**, 333–366 (2016).
6. I.D. Donato and G. Lazzara, Porosity determination with helium pycnometry as a method to characterize waterlogged woods and the efficacy of the conservation treatments. *Archaeometry* **54**, 906–915 (2012).
7. R. Moriana, F. Vilaplana, S. Karlsson, and A. Ribes, Correlation of chemical, structural and thermal properties of natural fibres for their sustainable exploitation. *Carbohydr. Polym.* **112**, 422–431 (2014).
8. J.L. Guimarães, F. Wypych, C.K. Saul, L.P. Ramos, and K.G. Satianarayana, Studies of the processing and characterization of corn starch and its composites with banana and sugarcane fibers. *Carbohydr. Polym.* **80**(1), 130–138 (2010).
9. L. Segal, J.J. Creely, A.E. Martin Jr., and C.M. Conrad, An empirical method for estimating the degree of crystallinity of native cellulose using the X-ray diffractometer. *Text. Res. J.* **29**, 786–794 (1959).
10. A.P. Barbosa, http://uenf.br/posgraduacao/engenharia-de-materiais/wp-content/uploads/sites/2/2013/07/Tese-de-doutorado_fibras-de-Buriti_.pdf (2011).
11. A. Jordá-Vilaplana, V. Fombuena, D. García-García, M.D. Samper, and L. Sánchez-Nácher, Surface modification of polylactic acid (PLA) by air atmospheric plasma treatment. *Eur. Polym. J.* **58**, 23–33 (2014).
12. G.O. Berim and E. Ruckenstein, Nanodrop on a nanorough hydrophilic solid surface: Contact angle dependence on the size, arrangement, and composition of the pillars. *J. Colloid Interface Sci.* **359**(1), 304–310 (2011).
13. Y. Zhao, C. Xu, C. Xing, X. Shi, L.M. Matuana, H. Zhou, and X. Ma, Fabrication and characteristics of cellulose nanofibril films from coconut palm petiole prepared by different mechanical processing. *Ind. Crops Prod.* **65**, 96–101 (2015).
14. V. Fiore, T. Scalici, and A. Valenza, Characterization of a new natural fiber from *Arundo donax* L. as potential reinforcement of polymer composites. *Carbohydr. Polym.* **106**, 77–83 (2014).
15. M.M. Kabir, H. Wang, K.T. Lau, and F. Cardona, Effects of chemical treatments on hemp fibre structure. *Appl. Surf. Sci.* **276**, 13–23 (2013).
16. H.L. Ornaghi Jr., M. Poletto, A.J. Zattera, and S.C. Amico, Correlation of the thermal stability and the decomposition kinetics of six different vegetal fibers. *Cellulose* **21**(1), 177–188 (2014).
17. N. Nakayama and T. Hayashi, Preparation and characterization of poly(L-lactic acid)/TiO₂ nanoparticle nanocomposite films with high transparency and efficient photodegradability. *Polym. Degrad. Stabil.* **92**(7), 1255–1264 (2007).
18. P.N. Thanki, E. Dellacherie, and J-L. Six, Surface characteristics of PLA and PLGA films. *Appl. Surf. Sci.* **253**, 2758–2764 (2006).
19. A.P.B. Gonçalves, C.S. de Miranda, D.H. Guimarães, J.C. de Oliveira, A.M.F. Cruz, F.L.B.M. da Silva, S. Luporini, and N.M. José, Physicochemical, mechanical and morphologic characterization of purple banana fibers. *Mater. Res.* **18** (Suppl 2), 205 (2015).
20. N. Stevulova, J. Cigasova, A. Estokova, E. Terpakova, A. Geffert, F. Kacik, E. Singovszka, and M. Holub, Properties characterization of chemically modified hemp hurds. *Materials* **7**, 8131–8150 (2014).
21. S-l. Yang, Z-H. Wu, W. Yang, and M-B. Yang, Thermal and mechanical properties of chemical crosslinked polylactide (PLA). *Polym. Test.* **27**(8), 957–963 (2008).
22. Y. Wang, Y. Qin, Y. Zhang, M. Yuan, H. Li, and M. Yuan, Effects of N-octyl lactate as plasticizer on the thermal and functional properties of extruded PLA-based films. *Int. J. Biol. Macromol.* **67**, 58–63 (2014).
23. A. Awal, M. Rana, and M. Sain, Thermorheological and mechanical properties of cellulose reinforced PLA biocomposites. *Mech. Mater.* **80**, 87–95 (2015).
24. P.J. Jandas, S. Mohanty, and S.K. Nayak, Surface treated banana fiber reinforced poly(lactic acid) nanocomposites for disposable applications. *J. Cleaner Prod.* **52**, 392–401 (2013).
25. B. Wittbrodt and J.M. Pearce, The effects of PLA color on material properties of 3-D printed components. *Addit. Manuf.* **8**, 110–116 (2015).